International Journal of Steel Structures 17(2): 763-774 (2017)
DOI 10.1007/s13296-017-6030-8
ISSN 1598-2351 (Print)
ISSN 2093-6311 (Online)

International Journal of
STEEL
STRUCTURES
www.springer.com/journal/13296

Microstructure and Transverse Shrinkage Stress Analysis in GTA Welds of P91 Steel Pipe

Chandan Pandey[1,*], H. K. Narang[3], N. Saini[1], M.M. Mahapatra[2], and Pradeep Kumar[1]

[1]*Department of Mechanical and Industrial Engineering, Indian Institute of Technology Roorkee, Uttrakhand, 247667, India*
[2]*School of Mechanical Sciences, Indian Institute of Technology Bhubaneswar, Odisha, 751013, India*
[3]*Department of Mechanical Engineering, National Institute of Technology Raipur, Chhattisgarh, 492010, India*

Abstract

In a steam power plant, several components such as boiler tube, condenser and steam lines are made of high creep resistant steel. The P91 steel pipes are generally used in steam power plant because of high creep strength at service temperature of approximately 600°C. In the present research work, the study about shrinkage stresses and their distribution in the four quadrants of P91 pipe weld of 11 mm thickness is reported. The conventional-V and narrow-groove welds were prepared by using the gas tungsten arc welding (GTAW) process. Welding current, arc voltage, groove design, and straining length were the main parameters that affect the transverse shrinkage stresses. In the present research work, the effect of groove design on transverse shrinkage stresses has been evaluated. It also describes the effect of the number of passes on shrinkage. It is concluded that, for a given heat input, the narrow groove pipe weld joint exhibits comparatively less transverse shrinkage stress. Scanning electron microscope (SEM) with field emission gun and optical microscope has been used to characterize the weld fusion zone and HAZs of P91 pipe weldments.

Keywords: P91, transverse shrinkage stress, narrow-groove, V-groove, PAGBs

1. Introduction

Approximately 40% of the world electricity is produced by the steam power plants, where coal is used as the main source of energy, but global CO_2 and CO emissions are the main drawback of coal-fired power plants. The improvements in the efficiency of the coal-fired power plants have been limited owing to the environment conditions (Muramatsu, 1999; Staubli *et al*., 2003; Scheffknecht *et al*., 2003). The operating temperature and pressure of steam is used as the controlling parameters on which the efficiency of power plants depends. The steam temperature and pressure is limited by the operating material properties (Staubli *et al*. 2001; Scheu *et al*., 2005). In coal-fired power plants, the temperature of steam must be in the range of 550-650°C with pressure above 24 MPa. For Ultra Super Supercritical (USC), the coal-fired power plants modified 9Cr-1Mo (P91) steel because it is one of the primary materials for turbine and boiler component operating at high temperature (Abe *et al*., 2008; Blum and Vanstone, 2006), by the virtue of its superior mechanical and thermal properties at high temperature (Clarke *et al*., 2003; Hald, 2010; Vigneron *et al*., 1988).

P91 steel is an improved version of 9Cr-1Mo, titled as P91 for pipe, T91 for tube, and ASTM A335 for plate. The P91 steel is composed of high creep strength enhanced ferritic (CSEF) steel with approximately 9% of chromium. It also contains small amount of V, Nb, Mo and varying addition of Co, N and Ni. In this V, Nb and N were added for strengthening the solid solution. The increased volume fraction of fine MX precipitates and smaller particle to particle distance enhance the creep strength of P91 steel by pinning the free dislocations movement. During high temperature service condition, the fine MX precipitates enhance the creep strength by pinning the dislocation movement. Fine MX precipitates also refine the grain structure during normalizing and delays the plastic deformation (Shrestha *et al*., 2013). However, the laves and Z-phase precipitation may reduce the creep strength of P91 steel by dissolving the fine MX precipitates and by weakening the strength of the solid solution (Shrestha *et al*., 2015). It is widely used for power generating appliances such as superheater and reheater. In 1959s, the P91 steel was developed in Oak Ridge National Laboratory (ORNL) by a petrochemical plant.

Received July 28, 2016; accepted December 6, 2016;
published online June 30, 2017

*Corresponding author
Tel: +91-1332285518, Fax: +91-1332285665
E-mail: narangiitr@gmail.com, chandanpy.1989@gmail.com

The as-received material of P91 steel undergoes normalizing and tempering to obtain better mechanical properties. It is normalized in an austenite regime (1040-1100°C) and then cooled to room temperature. It enables the martensitic transformation during air cooling, and martensitic late structure is formed after normalizing. The steel is then subject to tempering, and martensitic lath structure is converted into subgrain structure. The microstructure of P91 steel has tempered martensitic structure that constitutes of finely dispersed precipitates of carbides, nitrides and carbonitrides along the sub-grain boundaries as well as grain interior region that provide optimum combination of strength and toughness (Hald, 2008; Pandey and Mahapatra, 2016a). In P91 steel, tempered martensite with randomly distributed laths make the slip difficult. The alloying elements, such as Fe, Cr, Mo, and Mn promote the formation of $M_{23}C_6$ and M_7C_3 type Cr-rich precipitates. Nb and V promote the formation of fine MX [M: V, Nb; X: C, N] type precipitates (Pandey *et al*., 2016a; Pandey *et al*., 2016b). The elongated rod-like or block-like Cr-rich $M_{23}C_6$ precipitates present in the microstructure, captured along the lath boundaries and the prior austenite grain boundaries (PAGBs), thereby improving the creep strength by pinning the boundaries and reducing the boundary migration. However, for long service condition at high-temperature, these favorable effects diminish. The microstructure degradation is the main factor responsible for loss in creep strength.

A considerable change in the mechanical properties of as-received P91 steel was observed during the manufacturing processes such as welding. The change in mechanical properties was observed because of the microstructure transformation, that is, from tempered martensite to untempered lath martensite. To obtain the desired microstructure, it is necessary to perform the post-weld heat treatment (PWHT) (Pandey and Mahapatra, 2016b). Joining of P91 pipe in industry is generally carried out by gas metal arc welding (GMAW) or gas tungsten arc welding (GTAW) with GTAW root pass (Han *et al*., 1999). During the multi-pass welding, the weld metal undergoes localized solidification shrinkage (Deng *et al*., 2008; Ghosh *et al*., 2007). The repetitive influence of thermal cycle from subsequent weld passes affect the development of stress in weld groove upto certain extent, and finally it causes continuous change in groove design and groove area with every weld passes (Dong, 2001; Kulkarn, 2008). Due to change in grove size with subsequent pass, the groove angle will also change, and it will not be uniform at all location in each quadrant of pipe. It is observed that the change in groove size and groove area is more in the case of V-groove welding than narrow-groove welding (Kulkarn, 2008). This occurred because of the present of less area at the narrow-groove (less weld metal deposition) than V-groove.

The solid phase transformation and welding boundary condition play crucial role in final stress distribution. Solid phase transformation occurs in two different manner. First one is formation of secondary phase particles during the heating process and second one is the transformation of matrix from one atomic packing to other during the heating and cooling process. The transformation occur during the heating and cooling cycle influence the formation of residual stress level. The character of the material is mainly responsible for the phase transformation. In P91 steel, the martensitic transformation occurs during the welding cycle whose effect is more complex and acts to influence the level of stress in transformed zone. Cottam *et al*. (2014) studied the effect of both type of phase transformation on stress formation. They had reported that the martensitic transformation is more complex and help to reduce the magnitude of stress in transformed zone. The point at which martensitic transformation starts results in an increase in stress level in adjacent non-deformed zone. Murkawa *et al*. (2008) had reported on the phase transformation effect on the stress. They had studied the effect of martensitic transformation temperature (M_s) on the nature and magnitude of residual stress. A low M_s-temperature is helpful to develop compressive stress component which reduces the magnitude of net tensile residual stress within the fusion zone. The magnitude of compressive stress was observed to be decreasing with the decrease in the M_s-temperature upto 200°C. The tensile nature of longitudinal stress developed in the heat affected zone is not affected by the M_s-temperature.

In the present investigation, an effort has been made to analyze the nature and distribution of transverse shrinkage stresses in different quadrants of P91 pipe weld during weld deposition in each lap by using GTAW. It is also reported that how the shrinkage stresses varies with number of passes. The procedural aspects of welding are changed with change in weld groove design from V-groove (14.58 mm opening) to narrow groove (9.06 mm opening).

2. Experimental Details

2.1. Material and filler wire

In the present study, the P91 steel pipe is used for the investigation. The as-received P91 steel pipe has outer diameter and thickness of a 60.3 and 11 mm, respectively. Before supplying, the base material is subjected to the austenitizing and tempering (austenitization-1040°C/10 min, air cooled and tempering-760°C/2 h, air cooled). Depending on the welding processes, the filler wire was selected by generally matching physical and chemical characteristic of the base metal. For GTAW, 9CrMoV-N (AWSER90S-B9) has been used as consumable. The chemical composition of P91 steel, weld metal, and consumable is depicted in Table 1. GTAW filler wire of diameter 1.6 and 1000 mm cut length was used for welding.

Table 1. Chemical composition of P91 pipe, 9CrMoV-N weld filler wire, and weld metal, wt. %

Element	Chemical composition (wt. %)												
	C	Mn	Cr	Si	Mo	V	Nb	Ni	N	S	Ti	W	Cu
Base metal	0.146	0.543	8.486	0.275	0.948	0.136	0.008	0.351	0.02	0.0114	0.0117	0.01	0.059
Filler metal	0.12	0.50	8.83	0.30	0.90	0.20	0.055	0.307	0.02	0.004	0.001	-	-
Weld metal	0.11	0.36	8.28	0.25	0.87	0.204	0.008	0.437	0.02	0.005	0.002	0.01	0.062

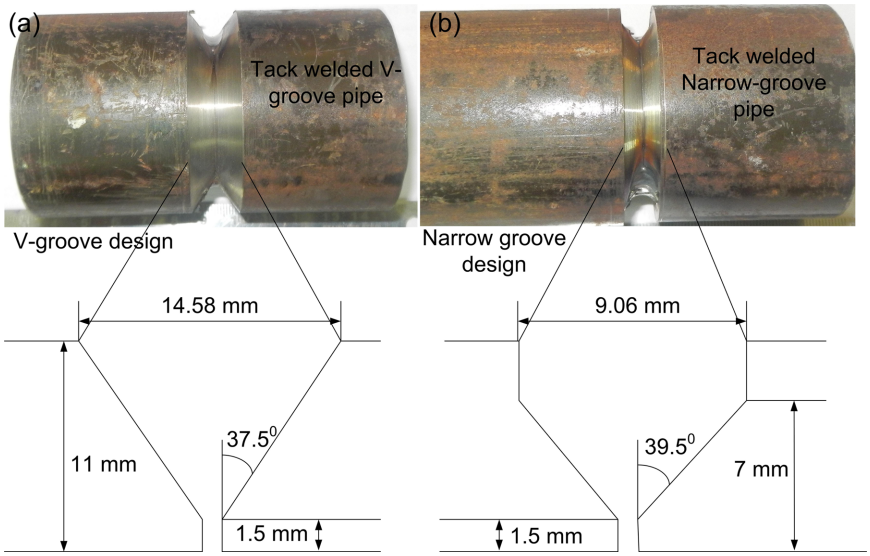

Figure 1. (a) Groove designs for conventional V-groove and narrow-groove, (b) Groove pipes after tack welding.

Table 2. Groove width and groove area before and after welding

Groove design	Groove area (mm^2)		Groove width (mm)		HAZ area (mm^2)	
	Conventional V-groove	Narrow groove	Conventional V-groove	Narrow groove	Conventional V-groove	Narrow groove
Before weld	69.25	63.40	14.58	9.06	-	-
After weld	118.48	81.42	17.11	11.59	90.58	92.96

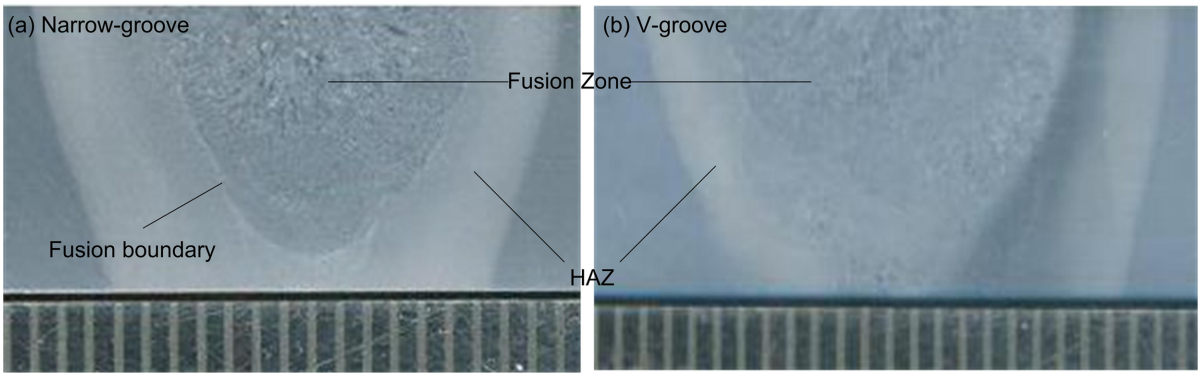

Figure 2. Macrograph showing the cross-section of weldment (a) Narrow-groove design, (b) V-groove design.

2.2. Groove design

For making the P91 pipe butt-joint, the conventional V-groove and narrow-groove designs are selected. The conventional V-groove and narrow grove designs is shown in Fig. 1. The P91 pipe after the tack welding is shown in Fig. 1. The groove opening and groove area for V-groove and narrow-groove weld design both before and after the welding is depicted in Table 2. The macro-structural overview of welded joint for V-groove and narrow-groove design is shown in Fig. 2. The HAZ area was calculated from a particular cut section of the welded pipe.

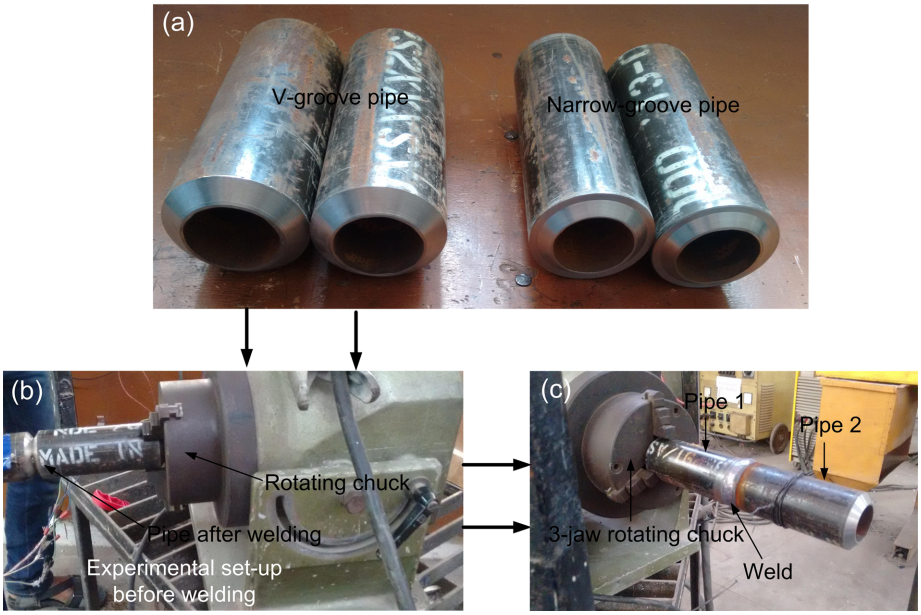

Figure 3. (a) V-grooved and narrow-grooved pipes, (b) tack-welded pipe joints with help of 3-jaw chuck, and (c) pipe joint after welding.

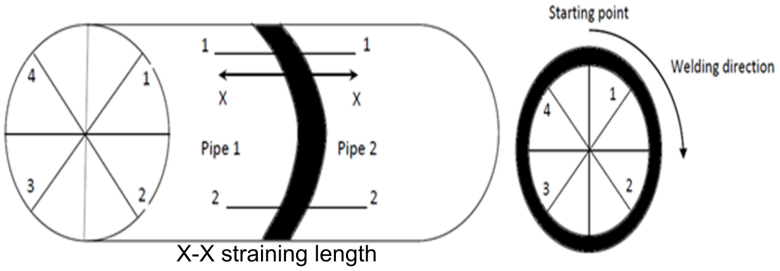

Figure 4. Schematic diagram of measurement of transverse shrinkage at different locations of pipe weld.

The P91 pipes of length 150 mm were multi-pass welded (8 passes: V-groove; 7 passes: narrow-groove) by using the gas tungsten arc welding (GTAW). The P91 pipe after groove preparation is shown in Fig. 3(a). The experimental set-up is shown in Fig. 3(b). The welding of pipe was performed on 1-GR position by holding the pipe in rotating table with the help of three jaws self-centering chuck. The mounted pipes in three jaws chuck before welding is shown in Fig. 3(b), and Fig. 3(c) shows the welded pipe joint.

2.3. Welding procedure and process parameter

After holding the pipes into three jaw chuck, the weld joint were prepared by autogenous GTAW root pass with current and voltages of 110 A and 12 V, respectively. The subsequent GTAW passes were carried out with welding current and arc voltages of 120 A and 12 V, respectively with electrode feed rate of 14.38 cm/min. Eq. (1) (Pandey *et al.*, 2016c) was used to calculate the heat input (KJ/cm) during welding process.

$$Q(KJ/mm) = \frac{V \times I \times \eta \times 60}{T} \quad (1)$$

where V=arc voltage, I=welding current, T=travel speed (mm/min), and η is arc efficiency taken as 0.75 in present work. Three samples for both V-groove and narrow-groove were welded. The possibilities of variation in groove size results from movement of groove wall in outer and inner direction, which may arise during welding due to direct and indirect effect of shrinkage of weld metal at different locations of pipe weld.

2.4. Measurement of shrinkage

The transverse shrinkage after each weld pass was estimated by using digital Vernier caliper having least count of 0.01 mm. It was estimated for the given initial straining length of 55 mm at four different quadrants of the pipe. After each weld pass, the transverse shrinkage was estimated at certain locations of four different quadrants along the entire circumference of pipe weld, as is schematically shown in Fig. 4.

2.5. Estimation of transverse shrinkage stress

The estimation of transverse shrinkage stress ($\sigma_{tr(i-j)}$) of a given location of pipe weld is generally considered as

a function of heat input and plate thickness (Kou, 2003; Panin, 2007).The transverse shrinkage developed during solidification of weld deposit in various quadrants is analyzed on the basis of variation in groove opening under different welding processes, procedures and parameters. It is calculated through the evaluation of transverse shrinkage, number of passes and average thickness of weld metal deposited per layer. It is given by (Ghosh *et al*., 2010);

$$\sigma_{tr(i-i)} = \frac{\Delta_{tr(msd)}}{N} \times \frac{a}{h} \times \frac{E}{L_s} \quad (1)$$

where,

$\Delta_{tr(msd)}$ = transverse shrinkage (mm)
N = number of weld layer
E = modulus of elasticity (GPa)
L_s = straining length (55 mm) (Fig. 4)
h = wall thickness of pipe
a = average thickness of weld metal deposited per layer

After calculating the transverse shrinkage stress ($\sigma_{tr(i-j)}$) at each location of the pipe weld, the average transverse shrinkage stress (σ_{avg}) generated in entire pipe weld were divided into the four quadrants along with its standard deviation which has been estimated as follows,

$$(\sigma_{avg}) = \sum_{i=0}^{4} \frac{\sigma_{tr(i-j)}}{4} \quad (2)$$

Standard deviation=

$$\sqrt{\left(\frac{1}{4} \times \sum_{i=0}^{4} (\sigma_{(i-j)} - \sigma_{avg})^2\right)} \quad (3)$$

Based on the estimation of transverse shrinkage stress at different location of pipe weld, the transverse shrinkage stress in each quadrant has been estimated by considering the average transverse shrinkage stress at the end point of any quadrant.

$$\sigma_{(i-j)} = \frac{\sigma_{i-i} + \sigma_{j-j}}{2} \quad (4)$$

3. Results and Discussion

3.1. Material

The mechanical properties of as-received P91 steel is given in Table 3. The standard metallographic techniques was used to prepare the sample for characterization. The sample was polished by using emery paper up to grit size of 2000 and etched with Vilella solution (100 mL of ethanol, 1 g of picric acid, and 5 mL of hydrochloric acid). The characteristics of the microstructure of P91 steel was examined by using SEMQUANTA 200 scanning electron microscope (SEM). Figure 5(a)-5(b) shows the typical micrograph of as-received P91 steel at different magnification.

In as-received condition, the P91 steel is characterized by tempered lath martensite, PAGBs, blocks, laths, sub-grains, packets, $M_{23}C_6$ precipitates, fine MX type precipitates and other precipitates (M_7C_3, Fe_3C, M_2X) (Pandey and Mahapatra, 2016c). The $M_{23}C_6$ mainly represents the general notation for $Cr_{23}C_6$, while Ni, Fe, Mo and Mn are also utilized as substitutes of Cr. In the early stage of precipitation, $M_{23}C_6$ undergoes a large compositional variation. Marshal *et al*. (1984) reported that in the early stage of tempering 40% Fe, countered in $M_{23}C_6$. The MX precipitates formation generally occurs due to strong carbide and nitride elements (Nb and V). The coarse $M_{23}C_6$ precipitates enhance the creep strength by resisting the movement of grain boundary and fine MX precipitates enhance the creep strength by pinning the movement of free dislocations. The $M_{23}C_6$ carbide precipitates are arrested along PAGBs and lath boundaries in the form of different morphologies and sizes ranging from 116 nm to 285 nm. The average precipitates size was reported about 138±49.5 (Pandey and Mahapatra, 2016c). At higher magnification, i.e. 50000x, the $M_{23}C_6$ particles accumulation along the PAGBs are clearly noticed in Fig. 5(b). The precipitates that beautify the PAGBs and grain interior region were examined by using energy dispersive X-ray spectroscopy (EDS). Figure 5(c)-5(d) represents the EDS spectra of coarse particles present at the PAGBs and fine particles present at the grain interior, respectively. The EDS spectra of coarse particles confirmed that the precipitates present at the PAGBs are enriched with Cr, Fe, and Mo, which are formed from the $M_{23}C_6$ precipitates as reported by Pandey *et al*. (2016a). The EDS spectra of fine precipitates at the grain interior region confirms the formation of fine $M_{23}C_6$ precipitates having less percentage of Mo, Cr, V and Nb in comparison to coarse $M_{23}C_6$ precipitates present at the PAGBs, which is indicated in Fig. 5(d).

3.2. Transverse shrinkage stress in conventional V-groove GTA welds

The transverse shrinkage $\Delta_{tr(msd)}$ was **e**stimated for different straining length of 55 mm at four different locations of pipe during welding for V-groove and narrow-groove in the same processes parameter. The value of shrinkage obtained during welding for different groove design is given in Table 4. In consideration of ($\Delta_{tr(msd)}$), the process of estimation of $\sigma_{tr(i-i)}$, σ_{avg}, and $\sigma_{(i-j)}$ for straining

Table 3. Mechanical properties of P91 steel plate in as-received condition

	Yield strength (MPa)	Tensile strength (MPa)	Elongation (%)	Hardness (HV)	Toughness (J)
P91 steel	475±25	715±15	20±2	247±4.6	200±8

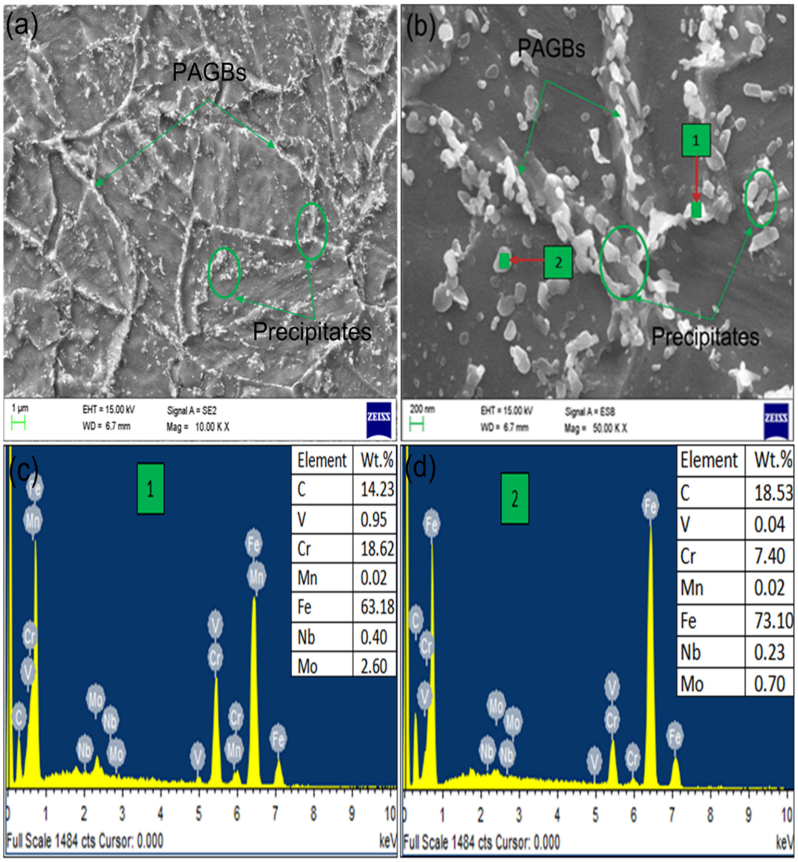

Figure 5. Microstructure of P91 steel in as-received state at different magnification: (a) 10000x, (b) 50000x, (c) EDS spectra of white particles presents at PAGBs (EDS spot 1), and (d) EDS spectra of white particles present at the grain interior (EDS spot 2)

Table 4. Measured transverse shrinkage at various locations of P91 pipe weld for different groove design and same welding condition for straining length of 55 mm

Sample	Type of Weld groove	No. of weld layer	Heat input (kJ/cm)	Estimated transverse shrinkage at various location of P91 pipe weld (mm)			
				1-1	2-2	3-3	4-4
1	Conventional V-groove	8	4.50	2.24	2.11	2.34	2.20
2				2.41	2.01	2.50	2.64
3				2.52	2.29	2.86	2.41
4	Narrow V-groove	8	4.50	1.47	1.52	1.63	1.38
5				1.68	1.55	1.89	1.80
6				1.52	1.37	1.49	1.49

length of 55 mm was typically presented in Table 5 for sample 1 (V-groove). The estimated transverse shrinkage stresses for conventional V-groove and narrow-groove design is given in Table 6. Table 6 shows a wide variation in the shrinkage stresses for different groove design.

Transverse shrinkage stress and their nature for V-groove developed during welding for the straining length of 55 mm and heat input of 6.005 KJ/Cm are given in Tables 7, 8, and 9 for the samples 1, 2, and 3, respectively. Table 7 reveals that for sample 1 of V-groove, the transverse shrinkage stresses present in the quadrants of 1-2, 4-1 are of tensile mode and those present in the quadrants of 2-3, 3-4 are of compressive mode. The average transverse shrinkage stress for the three samples is approximately 164.33 MPa as per our estimation.

3.3. Transverse shrinkage stress in narrow groove GTA welds

The variation of nature and magnitude of transverse shrinkage stresses at different location of GTA welded narrow-groove pipe for heat input of 6.005 KJ/Cm are given in Tables 10, 11, and 12 for samples 4, 5, and 6,

Table 5. Estimation of the $\sigma_{(i\text{-}i)}$ and $\sigma_{(i\text{-}j)}$ for V-groove pipe weld prepared by GTAW process

Estimation of the $\sigma_{(i\text{-}i)}$	Estimation of the $\sigma_{(i\text{-}j)}$
$\sigma_{(1-1)}=\frac{2.24}{8}\times\frac{1.64}{11}\times\frac{210\times10^3}{55}=159.39$	$\sigma_{(1-2)}=\frac{\sigma_{(1-1)}+\sigma_{(2-2)}}{2}=\frac{159.39+152.88}{2}=156.13$
$\sigma_{(2-2)}=\frac{2.11}{8}\times\frac{1.67}{11}\times\frac{210\times10^3}{55}=152.88$	$\sigma_{(2-3)}=\frac{\sigma_{(2-2)}+\sigma_{(3-3)}}{2}=\frac{152.88+140.11}{2}=146.49$
$\sigma_{(3-3)}=\frac{2.34}{8}\times\frac{1.38}{11}\times\frac{210\times10^3}{55}=140.11$	$\sigma_{(3-4)}=\frac{\sigma_{(3-3)}+\sigma_{(4-4)}}{2}=\frac{140.11+171.81}{2}=155.96$
$\sigma_{(4-4)}=\frac{2.20}{8}\times\frac{1.80}{11}\times\frac{210\times10^3}{55}=171.81$	$\sigma_{(4-1)}=\frac{\sigma_{(4-4)}+\sigma_{(1-1)}}{2}=\frac{171.81+159.39}{2}=165.60$
Estimation of the $\sigma_{avg}=\left(\frac{159.39+152.88+140.11+171.81}{4}\right)=156.04$	
Estimation of S.D.= $\sqrt{\left(\frac{1}{4}\times(156.04-159.39)^2+(156.04-152.88)^2+(156.04-140.11)^2+(156.04-171.81)^2\right)}=\pm11.45$	

Table 6. Measured transverse shrinkage stress at various location of P91 pipe welds under different groove design and same welding condition for 55 mm straining length

Sample	Type of Weld groove	Heat input (kJ/cm)	Estimated transverse shrinkage stress at various location of P91 pipe weld, (MPa)				Avg+Std. Dev.
			1-1	2-2	3-3	4-4	
1	Conventional V-groove	6.005	159.39	152.88	140.1099	171.81	156.04±11.44
2			172.53	161.33	186.57	168.38	172.21±9.21
3			158.54	160.96	177.45	164.16	165.27±7.30
4	Narrow groove	6.005	89.65	112.30	111.54	119.75	108.31±11.24
5			125.37	107.60	123.00	113.24	117.30±7.21
6			107.49	93.91	109.25	110.54	105.30±6.66

Table 7 Distribution of transverse shrinkage stress at different quadrants of pipe weld prepared by using GTAW and V- groove (sample 1)

Weld location	Transverse Shrinkage stress (MPa)	Nature	Avg. Transverse Shrinkage stress+Std. Dev.
1-2	156.13	Tensile	156.04±6.75
2-3	146.49	Compressive	
3-4	155.96	Compressive	
4-1	165.60	Tensile	

Table 8 Distribution of transverse shrinkage stress at different quadrants of pipe weld prepared by using GTAW and V- groove (sample 2)

Weld location	Transverse Shrinkage stress (MPa)	Nature	Avg. Transverse Shrinkage stress+Std. Dev.
1-2	166.93	Compressive	172.20±3.92
2-3	173.95	Tensile	
3-4	177.47	Tensile	
4-1	170.45	Compressive	

respectively. Table 10 reveals that the nature of transverse shrinkage stresses for sample 4 present in the quadrants 3-4, 4-1 are of tensile mode and those present in the quadrants of 1-2, 2-3 are of compressive mode. The average transverse shrinkage stress for the three samples is approximately 110.30 MPa, as per our estimation. Hence, a drastic decrease was observed in the shrinkage stress for narrow groove weld design that is from 164.33 to 110.33 MPa. The shrinkage stress estimated for the V-groove design was approximately 34% of the yield strength of material, and for the narrow-groove was approximately 23% of the yield strength of material. Hence, it can be concluded that weld is safe against the transverse shrinkage stress.

Table 9 Distribution of transverse shrinkage stress at different quadrants of pipe weld prepared by using GTAW and V- groove (sample 3)

Weld location	Transverse Shrinkage stress(MPa)	Nature	Avg. Transverse Shrinkage stress+Std. Dev.
1-2	159.75	Compressive	164.77±5.25
2-3	169.20	Tensile	
3-4	170.80	Tensile	
4-1	159.35	Compressive	

Table 10. Distribution of transverse shrinkage stress at different quadrants of pipe weld prepared by using GTAW and Narrow groove (sample 4)

Weld location	Transverse Shrinkage stress(MPa)	Nature	Avg. Transverse Shrinkage stress+Std. Dev.
1-2	100.97	Compressive	108.30±5.78
2-3	111.92	Compressive	
3-4	115.64	Tensile	
4-1	104.70	Tensile	

Table 11. Distribution of transverse shrinkage stress at different quadrants of pipe weld prepared by using GTAW and Narrow V- groove (sample 5)

Weld location	Transverse Shrinkage stress(MPa)	Nature	Avg. Transverse Shrinkage stress+Std. Dev.
1-2	116.48	Compressive	117.30±1.52
2-3	115.30	Compressive	
3-4	118.12	Tensile	
4-1	119.30	Tensile	

3.4. Effect of number of passes on shrinkage

The variation in transverse shrinkage after each pass for both conventional V-groove and narrow-groove weld design is shown in Fig. 6. From Fig. 6, it was observed that after each passes shrinkage will increase for both the groove designs, i.e., increase in shrinkage stress. From Fig. 6, it is clear that the transverse shrinkage measured in narrow-groove is much less than conventional V-groove design.

Table 12. Distribution of transverse shrinkage stress at different quadrants of pipe weld prepared by using GTAW and Narrow V- groove (sample 6)

Weld location	Transverse Shrinkage stress(MPa)	Nature	Avg. Transverse Shrinkage stress+Std. Dev.
1-2	100.7	Compressive	105.30±4.183
2-3	101.58	Compressive	
3-4	109.90	Tensile	
4-1	109.02	Tensile	

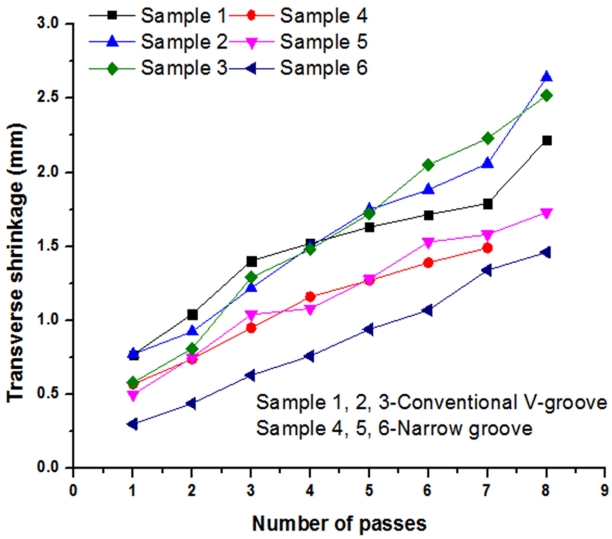

Figure 6. Cumulative shrinkage in conventional TIG and narrow TIG welds (Sample 1, 2, 3-conventional V-groove and Sample 4, 5, 6-Narrow groove)

3.5. Material characterization

The microstructure of the different zone of welded pipe joint of P91 steel along the axis normal to fusion line from weld metal to heat affected zone (HAZ) is shown in Fig. 7. Figure 7(a)-7(e) shows the optical micrograph of the various zone of P91 pipe weldments having a good agreement with micrograph obtained by Wu *et al*. (2004). The fusion boundary between weld and HAZ is shown in Fig. 7(a). The optical micrograph of weld fusion zone is shown in Fig. 7(b). The weld fusion zone is characterized with the untempered lath martensitic microstructure. After the fusion boundary, coarse-grained heat affected zone (CGHAZ) is observed. The approximate width of

Table 13. Hardness in various Zones of welded pipe and base metal before and after PWHT

Groove design		Weld	CGHAZ	IC-HAZ	Base metal
V-groove	As-welded	478±6	481	238	247±4
Narrow groove	As-welded	465±8	481	226	-

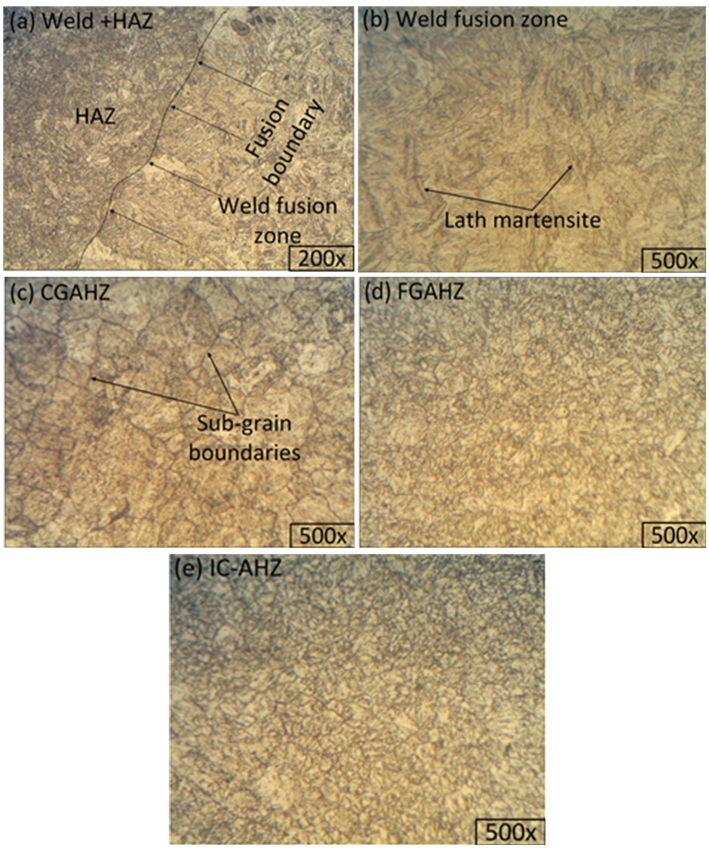

Figure 7. Microstructure of various zones of welded pipe.

CGHAZ was 1.2 and 1 mm for V-groove and narrow-groove, respectively. The maximum hardness of P91 pipe weldments occurred in the CGHAZ, i.e. 481 HV. The CGHAZ consisted of coarse austenite grains with almost no precipitation along the PAGBs and in the grain interior region. As depicted in Fig. 7(d), next to CGHAZ is the fine-grained heat affected zone (FGHAZ). The approximate width of FGHAZ was 4.6 and 3.6 mm for V-groove and narrow-groove welds, respectively. The hardness of each zone for both the groove designs is depicted in Table 13. The grain size measured in CGHAZ was about 277 μm. The soft zone present in P91 weld joint is inter-critical heat affected zone (IC-HAZ), as shown in Fig. 7(e). The grain size measured in IC-HAZ about 14±4 μm. The minimum size of grain was observed in FGHAZ about 11±3.65 μm.

The SEM image of weld fusion zone and HAZs of P91 steel weldments is presented in Fig. 8. The weldments consists of weld fusion zone, CGHAZ, FGHAZ and finally most interesting region of IC-HAZ. The weld fusion zone is characterized with untempered lath martensitic structure, as shown in Fig. 8(a). The lath martensite in the form of packets and blocks were formed inside the PAGBs. The PAGBs and lath martensite are clearly shown in Fig. 8(a). In CGHAZ, there is almost no grain boundary precipitation, because at high temperature precipitates which restrict the growth of austenite grains dissolve completely. The dissolution of precipitates increased the solid solution strengthening because of presence of C and N in solution. This results**,** the formation of lath martensite in CGHAZ region, as shown in Fig. 8(b) and introduce maximum hardness comparison to all other HAZ regions.

In the FGHAZ, the temperature is low and just above the transformation temperature $A_{c3}$and it is not enough to dissolve the precipitates completely. Hence, precipitates were observed in FGHAZ. The precipitates and PAGBs in FGHAZ are clearly denoted in Fig. 8(c). These undissolved particles are helpful to limit the austenite growth by pinning it. The tendency to form soft zone in P91 steel weldments are most interesting. In the ICHAZ region, the martensite formed in ICHAZ region does not show lath morphology because the austenite formed in the IC-HAZ is lean in C. The PAGBs and precipitates observed in IC-HAZ are denoted in Fig. 8(d).

The area selected for elemental mapping and EDS spectra in weld and HAZ is shown in Fig. 9(a). The EDS spectra of selected area of weld fusion zone indicate the presence of Cr and Fe precipitates, as shown in Fig. 9(b). From EDS spectra of weld fusion zone it might be observed that $M_{23}C_6$ particles present in weld fusion zone are enriched with Fe and Cr. The EDS spectra of selected area of HAZ zone indicates the presence Cr, Fe, Mo, Ni and V precipitates. Hence, it might be said that the $M_{23}C_6$ particles present in HAZ zone are enriched with Fe, Cr,

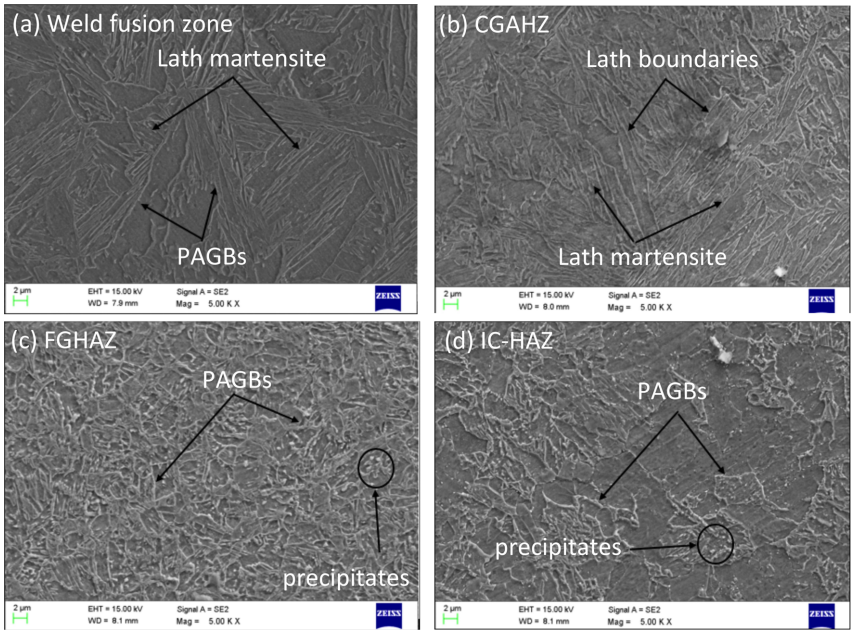

Figure 8. Scanning electron micrograph of various zone of P91 pipe weldments.

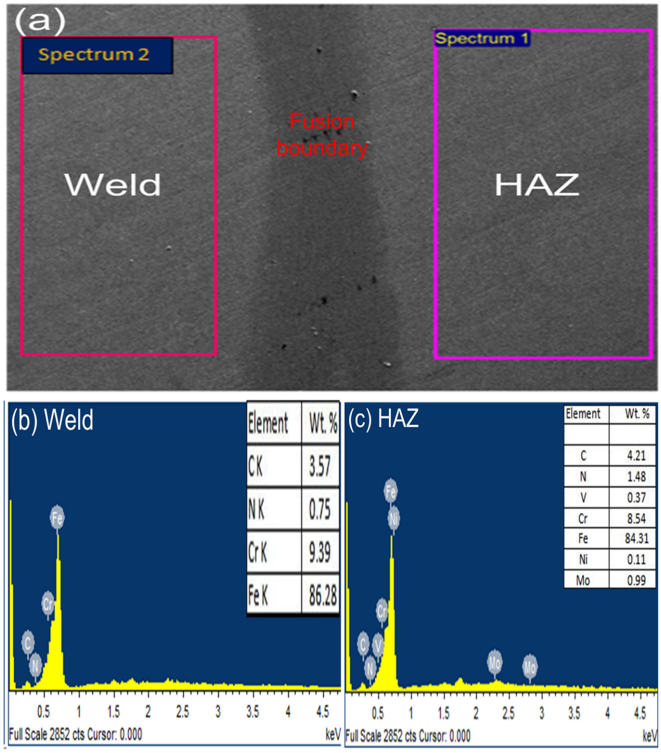

Figure 9. (a) Selected area in weld and HAZ zone for EDS spectra and elemental mapping, (b) EDS spectra of weld fusion zone, (c) EDS spectra of HAZ

and Mo. Presence of V indicates the formation of fine MX type precipitates.

The X-ray elemental mapping was performed to quantify the distribution and concentration of individual elements contained in weld fusion zone and HAZ. As shown in Fig. 10, EDS elemental mapping clearly reveals that the elements Fe, Cr, V, Nb, Mn, Mo, C, N, and Ni, were evenly distributed throughout weld fusion zone and HAZ.

Figure 9(b) indicates the presence of Fe, C, and Cr as the major chemical components with weight percentage of 86.28, 3.57, and 9.39%, respectively, over the entire region of the weld fusion zone. From elemental mapping, as shown in Fig. 10, it was confirmed that Fe, Cr, Mo and V elements have high concentration throughout the

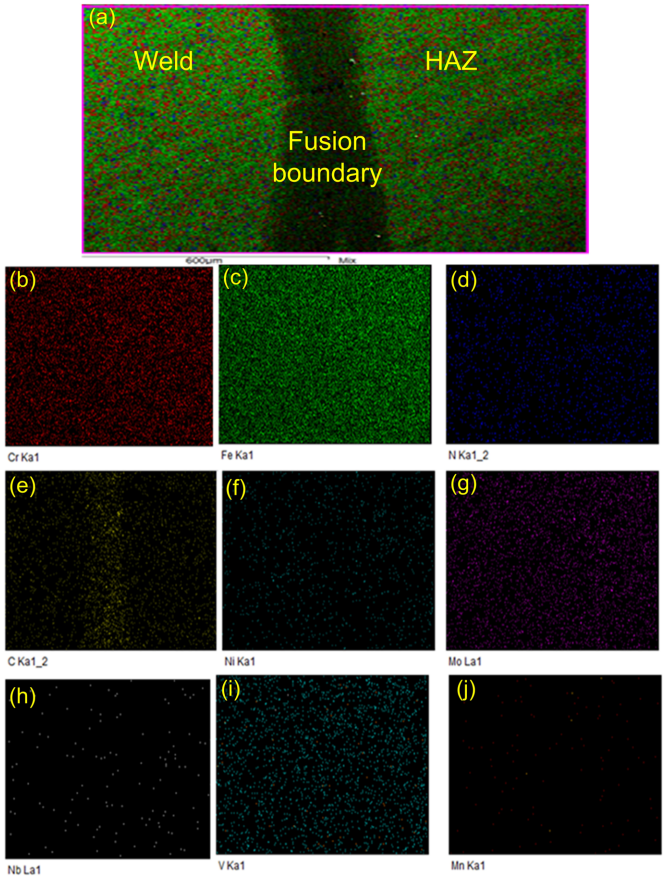

Figure 10. EDS elemental mapping data in weld fusion zone and HAZ (a) all displayed element, (b) Cr, (c) Fe, (d) N, (e) C, (f) Ni, (g) Mo, (h) Nb, (i) V, (j) Mn

weldments (weld fusion zone +HAZ). The elements C, N and Ni has lower concentration throughout the weldments. Nb and Mn have very low concentration throughout the weldments, as shown in Fig. 10(h) and 10(j), respectively. Fig. 10(a) indicates the uniform distribution of elements throughout the weldments.

4. Conclusions

(1) The average transverse shrinkage stress was estimated for the conventional V-groove and narrow groove design of 11 mm thick P91 pipe. The shrinkage stress estimated for V-groove and narrow groove weld design was 164.33 and 110.33 MPa, respectively. The transverse shrinkage stress estimated for V-groove design was approximately 34% of the yield strength of material and for narrow-groove was approximately 23% of the yield strength of material. Hence, it can be concluded that weld joint is safe against the transverse shrinkage stress.

(2) The mode and magnitude of transverse shrinkage stresses developed in each quadrant of pipe is different from each other for both the groove design.

(3) Transverse shrinkage after each pass increases. Transverse shrinkage develops in narrow groove is much less than that of conventional V-groove.

References

Abe, F., Kern, T. U., and Viswanathan, R. (2008). "Creep-resistant steels.", *Woodhead Publishing, CRC Press Cambridge*, England.

Blum, R., and Vanstone, R. W. (2006). "Materials development for boilers and steam turbines operating at 700°C." *Proc. 8th Liege Conf. Materials for Advanced Power Engineering, Liege,* Belgium, pp. 41-60.

Clarke, P. D., Morris, P. F., Cardinal, N., and Worral M. J. (2003). "Factors influencing the creep resistance of martensitic alloys for advanced power plant applications." *Proc. 6th Intern. Charles Parsons Turbine Conf.,* Maney Dublin, pp. 333-345.

Cottam, R., Luzin, V., Thorogood, K., Wong, Y.C., and Brandt, M. (2014). "The role of metallurgical solid state phase transformations on the formation of residual stress in laser cladding and heating." *Materials Science Forum,* 777, pp. 19-24.

Deng, D., Murkawa, H., and Liang, W. (2008). "Numerical and Experimental investigation of residual stress in multi pass butt welded austenitic steel pipe." *J. Mater. Sci*., 42, pp. 233-244.

Dong, P. (2001). "Residual stress analysis of a multi pass girth weld: 3-D special shell versus axis symmetric models." *J. Press.Vessel Tech*., 123, pp. 207-213.

Ghosh, P. K., Kulkarni, S. S., and Vaze, K. K. (2007).

"Superiroty of Narrow gap SMA Welding of 304LN stainless pipe." *Indian Weld. J.*, pp. 44-57.

Ghosh, P. K., Kumar, R. R., and Devakumaran, K. (2010). "Analytical studies on shrinkage stress distribution in GMA and pulse current GMA welds of thick wall stainless steel pipe having narrow and V-groove design." *Indian Weld. J.,* pp. 14-24.

Hald, J. (2010). "Development status and future possibilities for martensitic creep resistant steels." *Proc. 9th Liege Conf. Materials for Advanced Power Engineering,* Liege, Belgium, pp. 55-66.

J. Hald, "Microstructures and long term creep properties of 9-12% Cr steels." *Int. J. Press. Vessels Pip*., 2008, 85, pp. 3-37.

Han, H. Y., and Sun, Z. (1999). "Development of welding wire for high purity austenitic steels." *Welding J*., 78(2), pp. 38-44.

Kulkarni, S. (2008). "Narrow gap pulse current GMAW of thick 304LN stainless steel pipe." Ph.D Thesis, Metallurgical and Materials Engineering Department, IITRoorkee.

Kou, S. (2003). "Welding Metallurgy" Edition 2, A john Wiley & sons Interscience publication, pp. 122-130.

Muramatsu, K. (1999). "Advanced Heat Resistant Steel for Power Generation." University Press Cambridge Great Britain.

Murakawa, H., Beries, M., Vega, A., Rashed, S., Davies, C. M., Dye, D., and Nikbin, K. (2008). "Effect of phase transformation on set temperature on residual stress in welded thin steel plates." *Trans. JWRI,* 27(2), pp.75-80.

Marshall, P. (1984). "Austenitic stainless steel, microstructure and mechanical properties." Londan, Elsevier.

Pandey, C., and Mahapatra, M. M. (2016a). "Effect of heat Treatment on microstructure and hot impact toughness of P91 welded pipes." *J. Mater. Eng. Perform.,* 25(6), pp. 2195-2210.

Pandey, C., Giri, A., and Mahapatra, M. M. (2016a). "Evolution of phases in P91 steel in various heat treatment condition and their effect on microstructure stability and mechanical properties." *Mater. Sci. Eng. A*, 664, pp. 58-74.

Pandey, C., Giri, A., and Mahapatra, M. M. (2016b). "Effect of Normalizing Temperature on Microstructural Stability and Mechanical Properties of Creep Strength Enhanced Ferritic P91 Steel." *Mater. Sci. Eng. A*, 2016, 657, pp. 173–184.

Pandey, C., and Mahapatra, M. M. (2016b). "Effect of groove design and post-weld heat treatment on microstructure and mechanical properties of P91 steel weld." *J. Mater. Eng. Perform*., 25, pp. 2761-2775.

Pandey, C., and Mahapatra, M. M. (2016c). "Effect of long-term ageing on the microstructure and mechanical properties of creep strength enhanced ferritic P91 steel." *T Indian I Metals*, DOI: 10.1007/s12666-015-0826-z.

Pandey, C., Giri, A., and Mahapatra, M. M. (2016c). "On the prediction of effect of direction of welding on bead geometry and residual deformation of double-sided fillet welds." *Int. J. Steel Structure*, 16(2), pp. 333-345.

Panin, V. N. (2007). "Experimental Calculation estimation of Residual Welding Distortion in shell of turbine penestocks at hydraulic power stations." *Thepaton Weld. J.*, pp. 7-11.

Staubli, M., Scarlin, B., Mayer, K. H., Kern, T. U., Bendick, W., Morris, P., and Cerjak, H. (2003). "Materials for Advanced Steam Power Plants." The European COST 522 Action, *Proc. 6th Intern. Charles Parsons Turbine Conf.,* Maney Dublin, pp. 305–324.

Scheffknecht, G., Chen, Q., and Weissinger, G. (2003). "Design and Materials Aspects of Advanced Boilers." *Proc. 6th Intern. Charles Parsons Turbine Conf.,* Maney Dublin, 2003, pp. 114-128.

Staubli, M., Mayer, K. H., Kern, T. U., Vanstone, R. W., Hanus, R., Stief, J. and Schönfeld, K. H. (2001). "Cost 522 - Power Generation into the 21st Century." *Proc. Advanced Steam Power Plant,* University of Wales and EPRI, 2001, pp.15-32.

Scheu, Kauffmann, C., Zies, F. G., Maile, K. S., Straub, and Mayer, K. H. (2005). "Requirements for microstructural investigations of steels used in modern power plants." *J. Z. Metallkd.*, 96, pp. 653-659.

Shrestha, T., Basirat, M., Charit, I., Potirniche, G. P., and Rink, K. K. (2013). "Creep rupture behavior of Grade 91 steel." *Mater. Sci. Eng. A*, 565, pp. 382–391.

Shrestha, T., Alsagabi Sultan, F., Indrajit, C., Gabriel, P., Potirniche P. P., and Michael, V. G. (2015). "Effect of Heat Treatment on Microstructure and Hardness of Grade 91 Steel." *Metals*, 5, pp. 131-149.

Vigneron, G., Vanderschaeghe, A., and Lecoq, J. (1988). "A metallurgical contribution to the industrial-development of 12% chromium martensitic steels for pressure-vessels." *Int. J. Press. Vessels Pip*., 32, pp. 389-413.

Wu, R., Sandstrom, R., and Seitisleam, F. (2004). "Influence of extra coarse grains on creep properties of 9 Percent CrMoV (P91) steel weldment." *Eng. Mater. Tech*., 126, pp. 87-94.